Pergamon

Int. J. Solids Structures Vol. 33, No. 23, pp. 3377–3398, 1996

0020-7683/96 $15.00 + .00

0020-7683(95)00183-3

MULTI-DEGREES OF FREEDOM MODEL FOR DYNAMIC BUCKLING OF AN ELASTIC–PLASTIC STRUCTURE

D. KARAGIOZOVA
Institute of Mechanics, Bulgarian Academy of Sciences, Acad. G. Bonchev Str. Bl. 4, Sofia 1113, Bulgaria

and

N. JONES
Impact Research Centre, University of Liverpool, Liverpool L69 3BX, U.K.

(*Received* 28 *March* 1995; *in revised form* 7 *August* 1995)

Abstract—The dynamic elastic–plastic buckling phenomenon is studied using a multi-degrees-of-freedom model which retains the influences of axial and lateral inertia and the effects of initial geometrical imperfections. The process of buckling is considered as a quasi-bifurcation of an elastic–plastic discrete system together with an analysis of the post-bifurcation behaviour.

A lower bound to the initial kinetic energy causing a quasi-bifurcation of the model is defined as the initial kinetic energy at the transition between the response, when governed only by a uniform compression, and a response which involves an overall bending as well as compression. The critical impact energy is defined as an energy causing a loss of dynamic stability of the model.

The final buckling shapes and the corresponding critical quasi-bifurcation times are determined for a model with a particular set of parameters and subjected to several impact masses having different initial impact velocities. The range of application of a quasi-static method of analysis for the considered model is discussed.

The initiation of buckling predicted by the model is compared with some experimental results on the high velocity collision of metal rods, reported previously in the literature. Copyright © 1996 Elsevier Science Ltd

NOTATION

c	elastic wave propagation speed
c_p	plastic wave propagation speed
m_1	total mass of the model, $m_1 = 8m$, where m is defined in Fig. 1(a)
p_i	dimensionless axial force at location i
r	L_1/L
t	time
t_{cr}	critical time of quasi-bifurcation
u_i	axial displacement at location i in Fig. 1(a,b)
v_0	initial velocity of the striker
$\bar{x}_{i\alpha}$	spring displacements in Fig. 1(c)
$x_{i\alpha}$	$\bar{x}_{i\alpha}/L$, eqns 4(a–e)
y_i	u_i/L, dimensionless axial displacements
z_i	ζ_i/L_1, dimensionless lateral displacements
z_i^*	$\bar{\zeta}_i/L_1$, dimensionless initial imperfections
E	Young's modulus
E_t	hardening modulus
$F_{i\alpha}$	spring forces (Fig. 1(c))
$F_{i\alpha}^Y$	spring forces at yield (Fig. 1(c))
K, K_t	spring characteristics in Fig. 1(c)
L, L_1	model parameters in Fig. 1(a)
M	mass of the striker
$\bar{M}_i$	bending moments
M_i	dimensionless bending moments, $\bar{M}_i/P_C L$
P_C	$KrL_1(2-\sqrt{2})$, static buckling load for the model
P_i	$F_{i1}+F_{i2}$, axial force at location i in Fig. 1(a,b)
$Q_{i\alpha}$	dimensionless spring forces, eqn (3)
$Q_{i\alpha}^Y$	$F_{i\alpha}^Y/P_C$, dimensionless spring forces at yield
T, T_b, T_c, T_k	total, bending, compressive and kinetic energies made dimensionless by dividing by $P_C L$

V_0	dimensionless initial velocity, eqn (A10)
λ	K_t/K, hardening ratio
μ	M/m_1, mass ratio
ξ_i	lateral displacement at location i (Fig. 1(a))
$\bar{\xi}_i$	initial imperfection at location i (Fig. 1(a))
ω_1	lowest lateral elastic vibration frequency of the model, eqn (A8a)
σ_0	material yield stress
τ	dimensionless time, eqn (2f)
$(\,)'$	$\partial(\,)/\partial\tau$

1. INTRODUCTION

Although numerous studies on the dynamic buckling of structures have been reported in the literature, a complete understanding of this complex phenomenon does not exist, especially for the behavior of inelastic structures. Dynamic buckling depends on many factors such as initial geometrical and material imperfections, material properties, elastic and plastic deformation history as well as interactions between the axial stress waves and the slower moving structural waves.

Most numerical studies have been published on particular structural problems, which, because of their complexity, often reveal little general understanding of the dynamic buckling phenomenon. Nevertheless, this topic is an important practical one because systems consisting of axially loaded tubes and rods are used throughout engineering and designers cannot predict when the efficient mode of dynamic progressive buckling may be replaced by a less efficient global buckling mode, or by dynamic plastic buckling at higher impact velocities. No theoretical analyses are available to predict these various transitions in the dynamic behaviour of elastic-plastic structures, although the individual phenomena have been studied by several authors (e.g. Jones (1989)).

A notable experimental study on the dynamic buckling of rods and tubes, subjected to high velocity axial impacts, was performed by Abrahamson and Goodier (1966) who determined the dependence of the critical buckling time and the final deformed shape on the impact velocity. Several analytical studies (Lee (1977, 1981a, 1981b)), which neglect axial inertia effects, have examined the stability and quasi-bifurcation of an elastic-plastic continuum when subjected to a stepwise axial velocity. An analytical criterion of quasi-bifurcation is proposed when plastic buckling occurs for this particular case. An experimental criterion for the initiation or non-initiation of buckling has been developed in a later study by Bell (1988) where buckling is presented in terms of the quasi-static plastic buckling of nonlinear struts and predicted as a function of the impact velocity and rod dimensions.

A more complete explanation of the entire buckling phenomenon could be achieved by examining the stability and quasi-bifurcation behaviour of a structure and performing a post-bifurcation analysis which retains the possibility that the growth of the bifurcated motion could be different from the initial one.

In order to provide some insight into the phenomenon of dynamic elastic–plastic buckling, an imperfection-sensitive two-degrees of freedom model (Jones and dos Reis (1980), Karagiozova and Jones (1992a, 1992b, 1993, 1995)) has been developed to explore various features when the dynamic buckling mode is the same as the static one. It was found that the dynamic buckling load of the model with small initial geometrical imperfections was larger than the associated static buckling load for pressure loadings having a sudden increase and remaining constant for an unlimited duration (Jones and dos Reis (1980)). This observation supported the apparently paradoxical conclusions of an earlier numerical study by Hartzman (1974) on a spherical dome and arises because of the different histories of the elastic–plastic deformations in the static and dynamic loading cases. It was also found that two different types of dynamic buckling develop and are known as direct and indirect buckling. More recent studies (Karagiozova and Jones (1992a, 1992b)) have examined the influence of the pulse duration and the pulse shape to examine more realistic dynamic loadings. It was observed that the effect of the pulse loading is important even for pulses having a duration which is comparable with the corresponding natural period of the

model vibration and that the imperfection sensitivity of the model becomes more significant as the pulse duration decreases. Karagiozova and Jones (1993, 1995) have examined the dynamic elastic–plastic buckling of the same two-degrees-of-freedom model when struck axially by a mass to idealise drop weight loadings and other practical situations. These studies reveal that the material elastic–plastic characteristics play an essential role in estimating the kinetic energies causing dynamic buckling of the model and show the importance of retaining the influence of material strain rate sensitivity in the basic equations.

The multi-degrees of freedom model proposed herein is used to study the phenomenon of dynamic elastic-plastic buckling when higher buckling modes are activated in the lateral displacement field. The model retains the influence of axial and lateral inertia effects and follows the entire deformation history including several phases of elastic and plastic loading, unloading and reloading.

The governing equations are solved using standard programme DGEAR (IMSL FORTRAN library) for stiff ordinary differential equations (Gear (1971)) and the entire response is obtained for a wide range of load parameters. Various characteristics of the dynamic behaviour of the model are examined and several features explored. A comparison is made between the model predictions and some experiments reported by Bell (1988).

The initiation of the dynamic buckling process is determined from the numerical results by using the quasi-bifurcation theory, which was introduced by Lee (1977, 1981a) and the post-bifurcation behaviour of the model is analysed until dynamic buckling occurs. It transpires that the overall response consists of two distinct phases of deformation: a uniform axial compression of the model followed by an overall bending and buckling. A sufficiently low initial kinetic energy can be absorbed by a uniform axial compression in the plastic range leaving no energy available for the bending phase when no quasi-bifurcation occurs. However, even if the initial kinetic energy is large enough to cause a quasi-bifurcation, then the response of the model may still remain stable due to a stiffness change after a partial elastic unloading of the model. Nevertheless, sufficiently high initial kinetic energies will cause an unstable model behaviour to develop after quasi-bifurcation.

2. BASIC EQUATIONS AND A CONCEPT OF STABILITY

The dynamic buckling phenomenon is studied using a multi-degrees of freedom model of an elastic-plastic column which is subjected to an axial impact by a mass M travelling with an initial velocity v_0, as shown in Figs 1(a,b). The model consists of four rigid weightless links of length L connected by springs simulating the elastic, linear strain hardening material properties in Fig. 1(c). The length L_1 is related to the thickness of an actual column and the model has stress-free initial imperfections $\bar{\xi}_i$ ($i = 1, 2, 3$). The total mass of the model is m_1 and is distributed as discrete masses $m = m_1/8$ at each end of a rigid link. It is assumed that the springs have identical force-displacement characteristics, as shown in Fig. 1(c). The equations of motion are developed assuming moderate changes in the geometry of the model so that $[(\xi_i+\bar{\xi}_i)-(\xi_{i-1}+\bar{\xi}_{i-1})]/L = \sin\theta_i \simeq \theta_i$, where $\xi_i+\bar{\xi}_i$ are the total lateral displacements at the respective locations i ($i = 1, 2, 3$). The axial displacements of the masses are u_i ($i = 0, 1, 2, 3, 4$), as shown in Figs 1(a, b) and the axial inertia of the masses is retained in the basic equations in addition to the lateral inertia.

The dimensionless equations of motion in the axial and the lateral directions may be written as

$$
\begin{aligned}
y_0'' &= p_0/\mu,\\
y_i'' &= 4(p_i - p_{i-1}), \quad i = 1,\ldots,4,\\
z_1'' &= 4\{-2M_1 + M_2 - (p_0+2p_1+p_2)(z_1+\bar{z}_1)/2 + (p_1+p_2)(z_2+\bar{z}_2)/2\},\\
z_2'' &= 4\{M_1 - 2M_2 + M_3 + (p_1+p_2)(z_1+\bar{z}_1)/2 - (p_1+2p_2+p_3)(z_2+\bar{z}_2)/2\\
&\quad + (p_2+p_3)(z_3+\bar{z}_3)/2\}.
\end{aligned}
$$

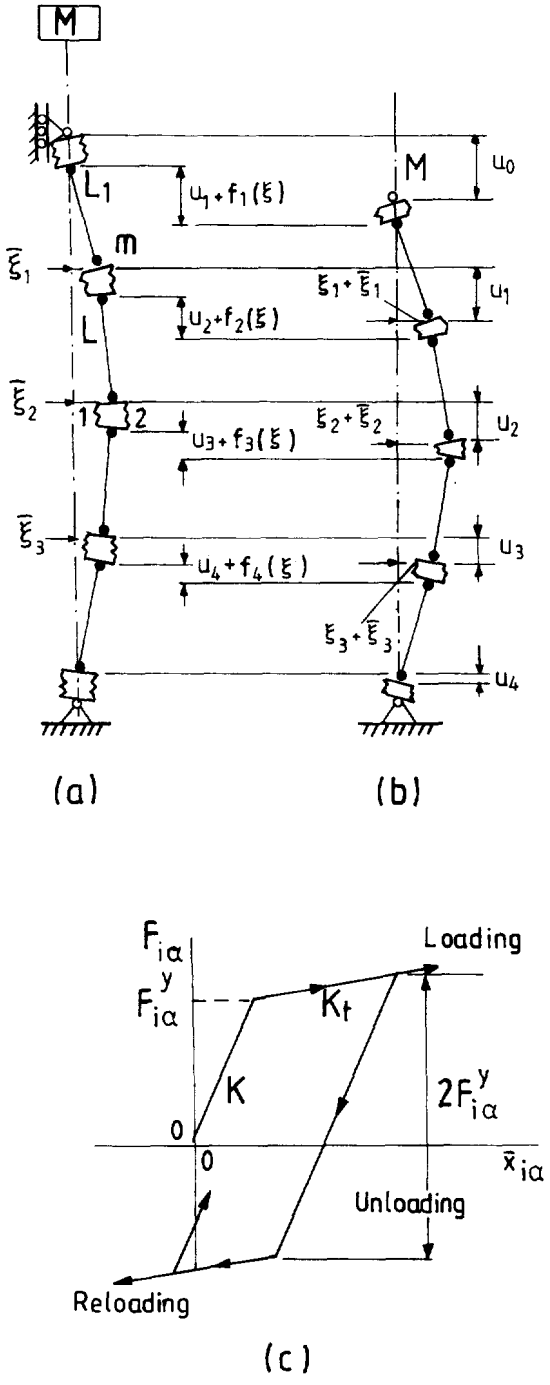

Fig. 1. Idealized model (a) initial position; (b) deformed position; (c) spring characteristics.

$$z_3'' = 4\{-2M_3 + M_2 + (p_2+p_3)(z_2+\bar{z}_2)/2 - (p_2+2p_3+p_4)(z_3+\bar{z}_3)/2\}, \qquad \text{(1a–h)}$$

where

$$y_i = u_i/L, \quad i = 0,\ldots,4; \quad r = L_1/L;$$
$$z_i = \xi_i/L_1, \quad \bar{z}_i = \bar{\xi}_i/L_1, \quad i = 1,2,3;$$
$$\mu = M/m_1; \quad \tau = [Kr^2(2-\sqrt{2})/m_1]^{1/2}t; \quad (\,)' = \partial(\,)/\partial\tau. \qquad \text{(2a–g)}$$

In eqns (1) $M_i = -(Q_{i1}-Q_{i2})/2$ are the dimensionless bending moments at each cell and

$p_i = P_i/P_C = (Q_{i1} + Q_{i2})$ are the associated dimensionless axial forces, where $Q_{i\alpha} = F_{i\alpha}/P_C$ ($i = 0, \ldots, 4$; $\alpha = 1, 2$)† are the dimensionless spring forces and $P_C = KrL_1(2-\sqrt{2})$ is the static buckling load (see eqn (A4a)).

The relationship between the dimensionless spring forces, $Q_{i\alpha}$, and the respective dimensionless spring displacements, $x_{i\alpha}$, may be expressed as

$$Q_{i\alpha} = Q^0_{i\alpha} + \psi_{i\alpha}(x_{i\alpha} - x^0_{i\alpha})/[(2-\sqrt{2})r^2], \quad \alpha = 1, 2, \quad i = 0, \ldots, 4, \tag{3}$$

where $\psi_{i\alpha}$ is a constant during each phase of elastic or plastic spring deformation. $\psi_{i\alpha} = 1$ for elastic behaviour when $Q^{min}_{i\alpha} \leqslant Q_{i\alpha} \leqslant Q^{max}_{i\alpha}$, where $Q^{max}_{i\alpha}$ is the largest dimensionless force in the previous plastic loading of spring ($i\alpha$), or the dimensionless yield force $Q^y_{i\alpha} = F^y_{i\alpha}/P_C$ when no plastic flow has occurred. $Q^{min}_{i\alpha}$ is the dimensionless yield force in compression $-F^y_{i\alpha}/P_C$ when no plastic reloading has occurred or the smallest dimensionless force in the previous plastic reloading. $\psi_{i\alpha} = \lambda = K_t/K$ when $Q_{i\alpha} \geqslant Q^{max}_{i\alpha}$ and $Q'_{i\alpha} \geqslant 0$ or when $Q_{i\alpha} < Q^{min}_{i\alpha}$ and $Q'_{i\alpha} < 0$, where $Q^{min}_{i\alpha} = Q^{max}_{i\alpha} - 2Q^y_{i\alpha}$. $Q^0_{i\alpha}$ and $x^0_{i\alpha}$ are the values of the forces and the displacements, respectively, at the end of each phase of plastic or elastic spring deformation. At $\tau = 0$, $Q^0_{i\alpha} = 0$ and $x^0_{i\alpha} = 0$.

The dimensionless displacements of the springs are

$$\begin{aligned}
x_{01} = x_{02} &= (y_1 - y_0) + f_1 r^2, \\
x_{1\alpha} &= (y_2 - y_1) + f_2 r^2 \pm (-2z_1 + z_2) r^2, \\
x_{2\alpha} &= (y_3 - y_2) + f_3 r^2 \pm (z_1 - 2z_2 + z_3) r^2, \\
x_{3\alpha} &= (y_4 - y_3) + f_4 r^2 \pm (z_2 - 2z_3) r^2, \quad \alpha = 1, 2, \\
x_{41} = x_{42} &= -y_4,
\end{aligned} \tag{4a–e}‡$$

where

$$\begin{aligned}
f_1 &= z_1(z_1 + 2\bar{z}_1)/2, \\
f_2 &= (z_2 - z_1)[z_2 - z_1 + 2(\bar{z}_2 - \bar{z}_1)]/2, \\
f_3 &= (z_3 - z_2)[z_3 - z_2 + 2(\bar{z}_3 - \bar{z}_2)]/2
\end{aligned}$$

and

$$f_4 = z_3(z_3 + 2\bar{z}_3)/2. \tag{5a–d}$$

It is assumed that the mass M strikes the model at the top end and after impact remains attached to the top cell.

The initial conditions for the problem posed (1–5) are

$$\begin{aligned}
&y_i(0) = 0, \quad i = 0, \ldots, 4, \\
&y'_0(0) = V_0, \quad y'_i(0) = 0, \quad i = 1, \ldots, 4, \\
&z_i(0) = 0, \quad \text{and } z'_i(0) = 0, \quad i = 1, 2, 3,
\end{aligned} \tag{6a–e}$$

where $V_0 = v_0 32\sqrt{6}/[\pi^2(2+\sqrt{2})^{1/2}cr]$ when assuming that the static buckling load of the model equals the Euler buckling load of a continuous column having the same slenderness ratio (see eqn (A10)). $c = (E/\rho)^{1/2}$ is the elastic wave speed in a continuous body having a density ρ. The shape of the initial imperfections is taken as $\bar{\xi}_i = \xi_0 \sin(\pi i/4)$, $i = 1, 2, 3$.

The process of dynamic buckling is determined from the numerical results by using the quasi-bifurcation theory introduced by Lee (1977, 1981a) together with an analysis of the post-bifurcation behaviour of the model.

† The summation convention is not used in this article.
‡ The + sign is used for $\alpha = 1$ and the − sign for $\alpha = 2$.

A quasi-bifurcation criterion for a class of systems, where the generalized forces are configuration dependent, was proposed by Lee (1977) in order to explain the buckling phenomenon within the plastic flow range. This criterion is based on the analysis of the time-dependent force field and determines the critical time, t_{cr}, when the effective force field around a dynamic path of an unstable system allows at least one perturbed motion, which oscillates initially within a small neighbourhood of the undisturbed trajectory, to depart monotonically from the neighbourhood. The properties of the effective force field around a stable trajectory must be such that

$$\zeta_r \ddot{\zeta}_r < 0 \quad \text{for } t > 0, \tag{7}$$

where ζ_r ($r = 1, \ldots, 8$) is the deviated motion $\Delta u_0, \ldots, \Delta u_4, \Delta\xi_1, \Delta\xi_2, \Delta\xi_3$ and $\ddot{\zeta}_r$ are the respective accelerations. The force field satisfying the inequality (7) for every ζ_r is called a restoring force field and, in general, is an oscillatory motion (Lee (1981a)). In such systems, the effective force field changes continuously in a domain $(t; \zeta_r, \dot{\zeta}_r)$ from a restoring force field ($\zeta_r \ddot{\zeta}_r < 0$), for $0 < t < t_{cr}$, and, for all ζ_r, to a diverging force field ($\zeta_r \ddot{\zeta}_r > 0$), for $t \geqslant t_{cr}$ at least for one ζ_r when at $t = t_{cr}$ a quasi-bifurcation occurs.

The bifurcation trajectory for $t > t_{cr}$ may be sensitive to the initial values of ζ_r and $\dot{\zeta}_r$. In fact, at $t > t_{cr}$, the new time-dependent force field may change the behaviour of the trajectories bringing them back to a new equilibrium state. If no equilibrium state of the trajectories $\zeta_r(t)$ is possible for $t > t_{cr}$ then the phenomenon of buckling of the model occurs. In the present study, the initial kinetic energy associated with an impact by mass M travelling with a critical velocity v_0^{cr}, which causes a transition between the stable model behaviour (which can be a new equilibrium state after a quasi-bifurcation) and an unstable one, is called a critical buckling energy.

3. RELATIONSHIP BETWEEN THE IDEALISED MODEL AND AN ACTUAL STRUCTURE

In this section relationships are given between the idealised model in Fig. 1 with $\xi_0 = 0$ (M) and an actual imperfection-free column (A) having a rectangular cross-section with width b^A, thickness $h^A = 2L_1$ and length $l^A = 4L^M$. The equality of the static buckling load for the model having $\xi_0 = 0$, P_C, and the Euler buckling load for a column and the equality of the fundamental lateral elastic vibration frequencies ω_1^M and ω_1^A are used as criteria for equivalency between the model and an actual structure.

The spring characteristic, K, is determined from the equality of the static buckling load for the perfect elastic model and the Euler buckling load for an actual column as

$$[KrL_1(2-\sqrt{2})]^M = (\pi^2 EI/l^2)^A, \tag{8}$$

which leads to

$$K^M = [\pi^2 EI/(h^2 l(2-\sqrt{2}))]^A, \tag{9}$$

where $I = (bh^3/12)^A$.

The spring yield forces $Q_{i\alpha}^y$ are determined by assuming that the total axial force $F_{i1} + F_{i2}$ corresponds to the force at yield present in a continuous column with a rectangular cross-section, $\sigma_0 A$, where σ_0 is the uniaxial yield stress and A is the total cross-section of the column. The dimensionless yield forces of the springs in the model presented in Figs 1(a,b) are

$$F_{i\alpha}^y/P_C = Q_{i\alpha}^y = 24\varepsilon_0/(\pi^2 r^2), \tag{10}$$

where $\varepsilon_0 = \sigma_0/E$ is the uniaxial yield strain and E is Young's modulus.

Equality of the first lateral vibration frequency of the model, ω_1^M (see eqn (A8a)), and the first vibration frequency of the actual structure ω_1^A, leads to an estimate of the mass of the model. Taking into account the corresponding formulae

$$(\omega_1^2)^M = \frac{K^M r^2}{m_1^M}\frac{8\sqrt{2}}{4+3\sqrt{2}} \quad \text{and} \quad (\omega_1^2)^A = \frac{\pi^4 EI^A}{(l^3 m)^A} \tag{11a,b}$$

together with eqn (9) the following relationship between the masses m_1^M and m^A is obtained

$$m_1^M = m^A 32/(\pi^2(2+\sqrt{2})). \tag{12}$$

The calculations in this paper are undertaken for a particular model which is made from a mild steel having $E = 200$ GPa, $\sigma_0 = 280$ MPa and $E_t/E = 0.005$, where E_t is the material strain hardening modulus. The influence of material strain-rate sensitivity is neglected in the present paper. A slenderness ratio of $h/l = 0.0125$ for a continuous column corresponds to the ratio $r = L_1/L = 0.025$ in the present model which has initial imperfections with a magnitude of $\xi_0 = 0.02L_1 = 0.01h$.

4. RESPONSE OF THE MODEL

The dynamic buckling of the model in Fig. 1 when it is struck at one end by a mass M travelling with an initial velocity, v_0, is a complex phenomenon due to inertia effects as well as the elastic–plastic material properties, material strain rate sensitivity and the influence of any initial imperfections. In the present study, emphasis is given to the influence of the inertia effects and elastic–plastic material properties of the model for a given set of initial imperfections and the influence of material strain rate sensitivity is neglected.

It transpires that two distinct phases of deformation are observed for the model over the range of the parameters examined in this paper. In general, the first phase of motion is a uniform axial compression which is followed by a second phase dominated by bending effects. For relatively low impact velocities, the compression phase is wholly elastic or elastic–plastic when only springs ($i1$) respond plastically while springs ($i2$) remain elastic. In these cases, quasi-bifurcation occurs in the elastic or elastic–plastic regimes, respectively. Sufficiently high impact velocities cause compressive plastic deformations in springs ($i2$) as well as in springs ($i1$) so that a quasi-bifurcation occurs in the plastic flow regime. Similar elastic–plastic and plastic–elastic buckling phenomena were observed by Jones and dos Reis (1980) and Karagiozova and Jones (1992b) for a two degrees of freedom model subjected to various types of pulse loadings. The experimental tests on low velocity axial impacts of a simple plate-structure performed by Tam and Calladine (1991) also show that the response of the structure has two separate phases of behaviour. In the first phase, a high compressive axial force develops in the specimen. The kinetic energy which remains in the striker at the end of this phase is absorbed in a second phase of motion by an overall bending of the specimen.

Figures 2(a,b) show the propagation of the axial compressive force in the model when it is struck by a mass having a mass ratio $\mu = 13$ with a dimensionless initial velocity $V_0 = 0.72$ ($v_0 \cong 20.94$ m/s). It is evident from Fig. 2(a) that axial inertia causes a delay in the spring responses which is analogous to the phenomenon of elastic wave propagation in a continuous body. The time for the compressive elastic force to propagate along the length of the particular model, $t_c = l/c$, can be expressed with the aid of eqn (A9) in terms of the dimensionless variables used for the model and is $\tau_c = 0.0237$ for the parameters considered herein. The speed of a plastic wave is $(\lambda)^{-1/2}$ times smaller than an elastic one, so the corresponding transmission time is $\tau_p = \tau_c(\lambda)^{-1/2} = 0.335$.

Figures 2(a,b) show that all the springs of the model in Fig. 1 have become plastic by the dimensionless time $\tau \cong 0.031$ and remain plastic until about $\tau \cong 0.52$, during the axial plastic compression phase (Fig. 2(b)). The bending moments shown in Fig. 2(c) remain

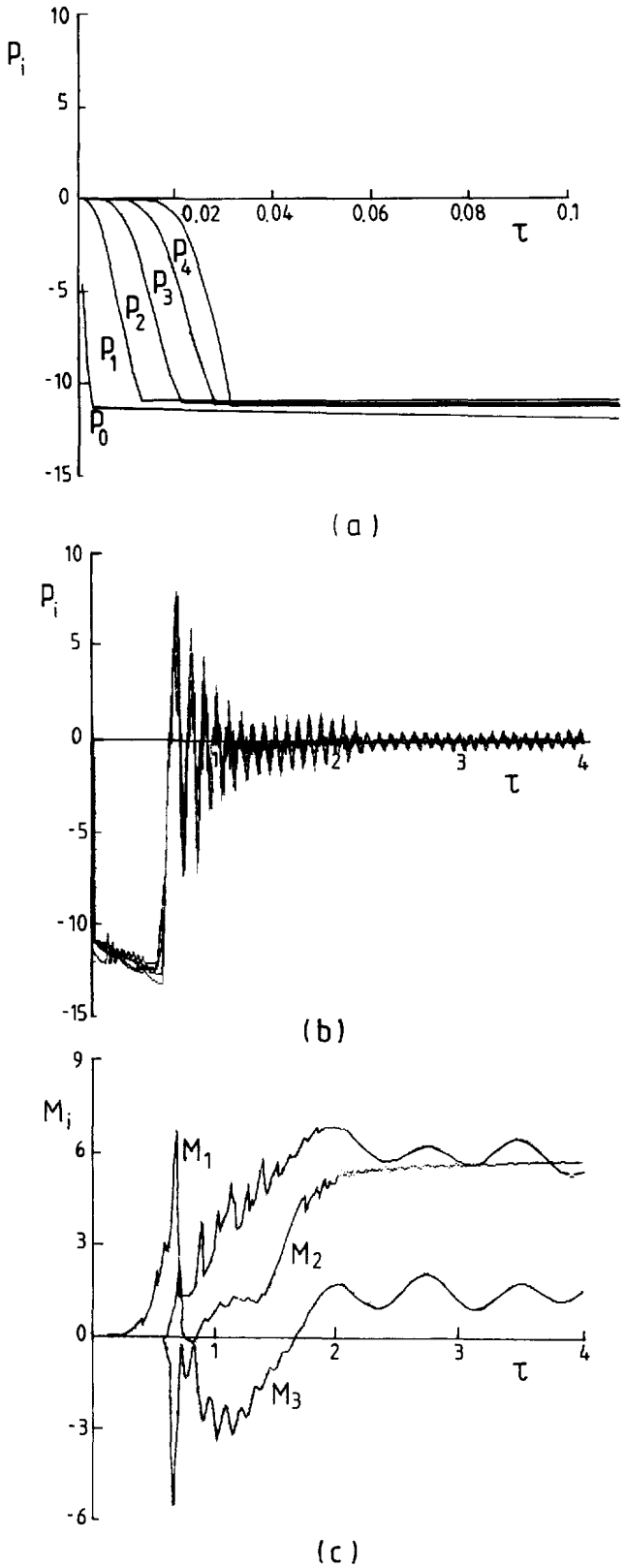

Fig. 2. Response of the model to an impact having $\mu = 13$ and $V_0 = 0.72$ ($r = 0.025$, $\lambda = 0.005$, $z_0 = 0.02$, $Q_{iz}^{\flat} = 5.447$). (a,b) Temporal variation of the dimensionless axial forces, p_i; (c) temporal variation of the dimensionless bending moments, M_i; (d) temporal variation of the dimensionless lateral accelerations, z_i''; (e) temporal variation of the dimensionless lateral displacements, ξ_{ii}/l; (f) temporal variation of the dimensionless lateral velocities, z_i'; (g) temporal variation of the dimensionless axial velocity, y_0'. (*Continued opposite and overleaf.*)

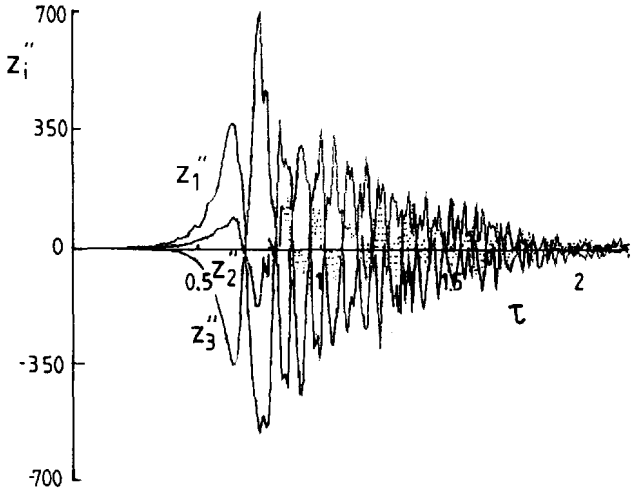

(d)

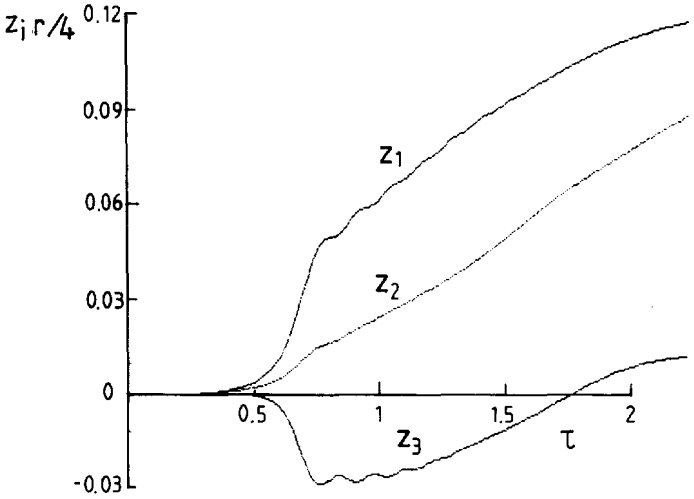

(e)

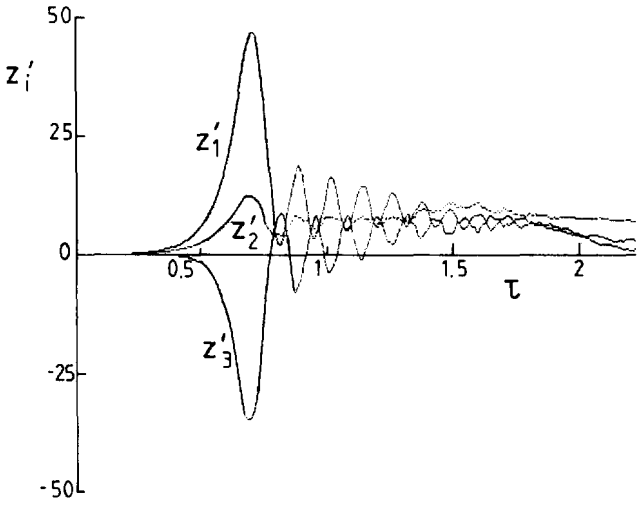

(f)

Fig. 2. *Continued.*

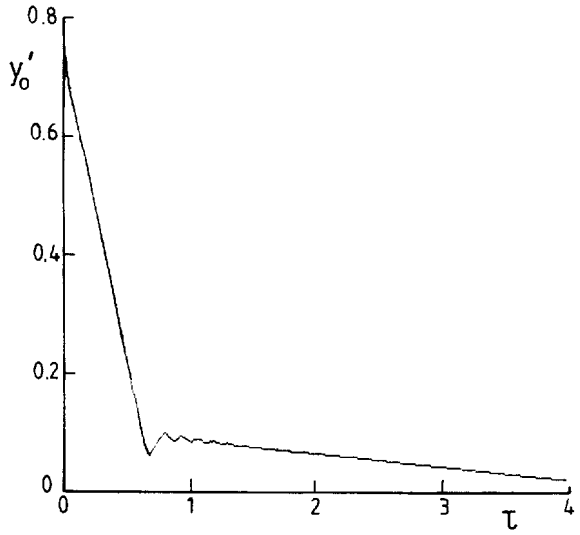

(g)

Fig. 2. *Continued.*

negligible until $\tau = \tau_{cr} \cong 0.32$, when following Lee (1977), a quasi-bifurcation of the trajectories z_i occurs. Thus, the behaviour of the model becomes unstable since criterion (7) is no longer satisfied and $z_i z_i'' > 0$ for all i until $\tau \cong 0.68$ (Fig. 2(d,e)). The accelerations z_i'' grow rapidly for $\tau > 0.32$ causing an overall or global deformation of the model with the corresponding deformations remaining in the plastic flow regime with no elastic unloading until $\tau \cong 0.52$. It turns out that, for these particular load parameters, the initiation of buckling starts within the plastic flow regime during the time of propagation of the primary plastic wave. The velocity profile (Fig. 2(f)) at quasi-bifurcation ($\tau_{cr} \cong 0.32$) characterizes the second buckling mode with a rapid growth of z_1 and a similar growth of z_3 but in the opposite direction, while z_2 grows more slowly (Fig. 2(e)). Around $\tau \cong 0.52$, the displacements become large enough to cause unloading of the springs (i.e., the spring ($i1$) may be in a phase of plastic reloading and spring ($i2$) in a phase of an elastic unloading). A rapid unloading of the model is observed between $\tau \cong 0.52$ and $\tau \cong 0.62$ when a considerable change in the model stiffness occurs due to the large value of the ratio K/K_l used in these calculations, which is, however, a realistic value for steel. The new stiffness characteristics of the model cause a significant change in the acceleration of the top end at $\tau \cong 0.58$, as indicated by the velocity-time history in Fig. 2(g). The further deformation of the model ($\tau > 0.58$) is governed largely by bending with a relatively small axial force.

The transformation of the initial kinetic energy during the deformation process is presented in Fig. 3(a). It is evident that at the beginning of deformation, the compression energy, T_c, increases rapidly reaching a maximum value at $\tau \cong 0.58$ and then remains constant during further deformation. The energy available for bending is $T_b = T-(T_c+T_k)$, where T is the initial kinetic energy and T_k is the kinetic energy of the striker at any time during the deformation process. It turns out that, in this particular case, the initial kinetic energy is not large enough to cause a loss of stability of the model, although it is sufficient to move the model to a new equilibrium position. The variations of the dimensionless axial displacement, u_0/l, at the top end of the model, together with the lateral displacements ξ_i/l, are shown in Fig. 3(b). Small elastic vibrations are observed around the new equilibrium state $\xi_1/l \cong \xi_2/l = 0.105$ and $\xi_3/l \cong 0$. In fact, the initial dimensionless velocity $V_0 = 0.72$ was found to be the critical impact velocity for an impact mass ratio $\mu = 13$ since a further increase of the impact velocity leads to an unstable model behaviour, as shown in Fig. 4 for $\mu = 13$ and $V_0 = 0.73$. Therefore, the final buckling shape† of the model at the critical

† For example, in Figs 3(b), 6(b) and 7 the final buckling shape is assumed to be given by the averages of the curves z_i–τ at large times.

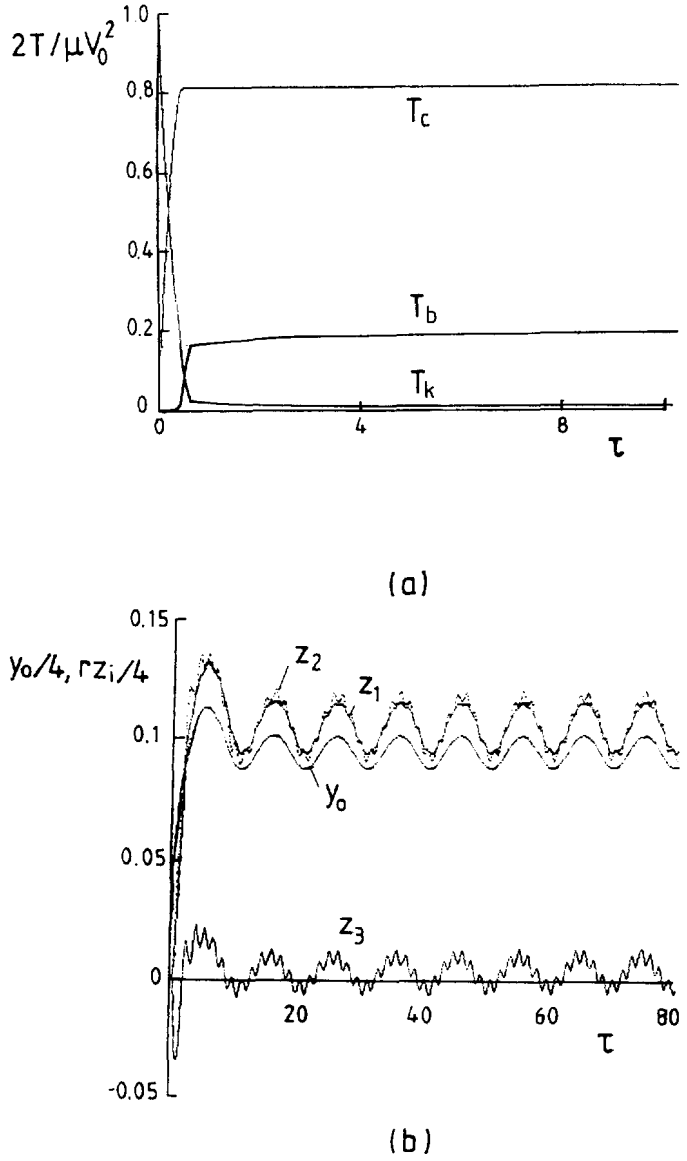

Fig. 3. Stable model response with $\mu = 13$ and $V_0 = 0.72$ ($r = 0.025$, $\lambda = 0.005$, $z_0 = 0.02$, $Q_b^* = 5.447$). (a) partition of the dimensionless energies in the model: T_k—dimensionless kinetic energy of the striker; T_c—dimensionless axial compression energy; T_b—dimensionless bending energy; (b) response of the model.

velocity has the characteristics of the second buckling mode with $\xi_1/l = 0.105$, $\xi_2/l = 0.105$ and $\xi_3/l \cong 0$ (Fig. 3(b)).

In certain circumstances, the initial kinetic energy can be absorbed entirely by axial compression with no energy available for the bending phase, as shown in Fig. 5(a) for $V_0 = 0.72$ and $\mu = 5.8$. It is evident from Fig. 5(b) that the lateral oscillations remain in a small neighbourhood of the initial undeformed position of the model, while the top end of the model oscillates in the neighbourhood of the axial compressive displacement, y_0. For the parameters mentioned above, the criterion $z_i z_i'' < 0$ is satisfied throughout the response and the response remains stable.

The two distinct axial compression and overall bending phases of deformation were observed for the entire range of impact mass ratios μ and impact velocities V_0 studied in this paper, although the buckling mode depends on the magnitude of the initial kinetic energy of the striker.

The development of the buckling modes for the model in Fig. 1 is presented in Figs 6 and 7. It appears that for dimensionless kinetic energies less than $\mu V_0^2/2 = 0.36$, which

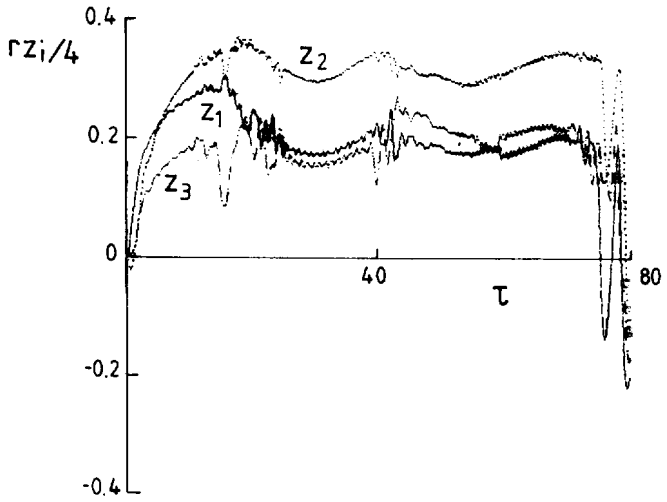

Fig. 4. Unstable model response with $\mu = 13$ and $V_0 = 0.73$ ($r = 0.025$, $\lambda = 0.005$, $z_0 = 0.02$, $Q_{in}^{*} = 5.447$).

corresponds to $\mu = 200$ and $V_0 = 0.06$ ($v_0 = 1.75$ m/s), the dynamic buckling mode is the same as the static one so that a quasi-static method of analysis would be adequate.

For mass ratios between $\mu \in (95, 200)$ bifurcation develops in the second buckling mode of the model within the plastic flow regime but changes, eventually, into the first mode of buckling where it remains to give the final buckling shape. A typical behaviour of the model at a low velocity impact is shown in Fig. 6 for $\mu = 100$ and a critical velocity $V_0 = 0.13$. The variation of the axial force, p_0, at the impacted end of the model is shown in Fig. 6(a) and remains elastic until $\tau = 0.066$. The time delay of the elastic force as it propagates down the different sections of the column is shown in Fig. 6(a). At $\tau \cong 0.1$, all of the spring forces along the entire length of the model have reached their elastic limit after which the compressive force increases slowly until $\tau \cong 0.58$ due to the slight material strain hardening effect. A quasi-bifurcation according to eqn (7) occurs at $\tau_{cr} = 0.4$, but the plastic bending deformations, z_3, are not large enough to support the initial second mode of buckling so that the deformations switch into a shape having the characteristics of the first mode which is then maintained for the remaining response. The temporal variation of the dimensionless axial displacements, u_0/l, and the lateral displacements, ξ_i/l, are presented in Fig. 6(b). The final buckling shape is associated with the equilibrium state $\xi_1/l = 0.118$, $\xi_2/l = 0.224$ and $\xi_3/l = 0.09$.

At a higher dimensionless impact velocity of $V_0 = 1.3$ for $\mu = 6$, quasi-bifurcation occurs in the third mode at the critical time $\tau_{cr} \cong 0.27$ and the subsequent deformation of the model remains in this mode. The temporal variations of the dimensionless axial displacement, u_0/l, and the dimensionless lateral displacements, ξ_i/l, are shown in Fig. 7. Apparently, after the initial formation of the plastic bending deformations, the inertia forces try to change the buckling shape of the model between $\tau = 2$ and $\tau = 12$ but the plastic deformations acquired during the earlier phase of bending are large enough to maintain a shape having the characteristics of the third buckling mode. The final equilibrium state of the model in Fig. 7 is characterized by the dimensionless lateral displacements $\xi_1/l = 0.11$, $\xi_2/l = -0.01$ and $\xi_3/l = 0.03$.

It was observed for the model in Fig. 1 that low velocity impacts with $V_0 < 0.06$ ($v_0 < 1.75$ m/s) and having a mass ratio $\mu \geqslant 200$ produce a dynamic buckling mode which has the same shape as that associated with static loads. Nevertheless, the results in Fig. 8 indicate that there is a considerable difference between the dynamic and the static energies required to obtain the critical buckling loads having the same buckling mode shapes. This difference arises because of the different elastic and plastic deformation histories of the springs. For critical velocities associated with impact mass ratios $\mu \in (200, 250)$, the axial compression involves plastic deformations of springs ($i1$) and ($i2$), so that a part of the initial kinetic energy is absorbed in compression and a quasi-bifurcation occurs in the

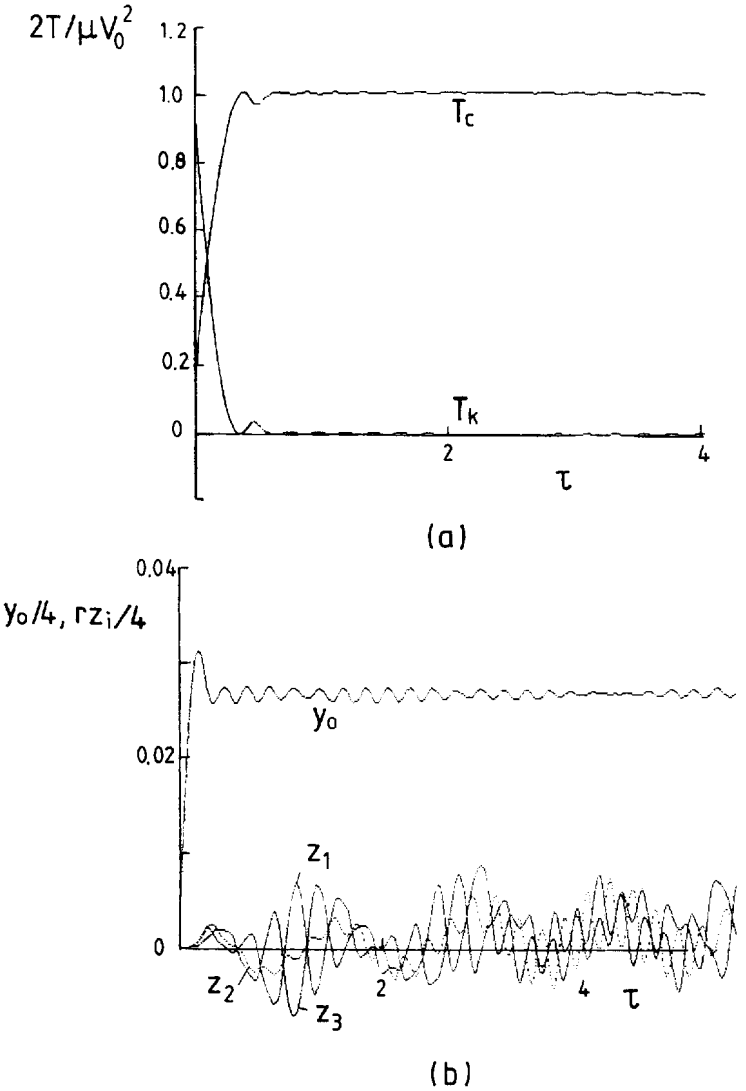

Fig. 5. Stable model behaviour at a lower bound to the initial kinetic energy corresponding to $\mu = 5.8$ and $V_0 = 0.72$ ($r = 0.025$, $\lambda = 0.005$, $z_0 = 0.02$, $Q_{cr}^{v} = 5.447$). (a) Partition of the energy in the model: T_k—dimensionless kinetic energy of the striker; T_i—dimensionless axial compression energy; (b) temporal variation of the dimensionless axial displacement u_0/l and the dimensionless lateral displacements, ξ_i/l.

plastic flow regime. The further growth of the bifurcated motion involves a partial unloading of the model followed by plastic loading in tension of spring (22), while spring (21) continues to load plastically in compression and the final deformed position of the model is characterized by small elastic vibrations around an equilibrium state having the first buckling mode shape.

Critical buckling energies corresponding to $\mu \in (250, 1200)$ and $V_0 \in (0.008, 0.025)$ cause plastic compression only in springs ($i1$), while springs ($i2$) do not reach the yield force value during the axial compression phase, so that only a small portion of the initial kinetic energy is absorbed in compression. Most of the initial kinetic energy is absorbed in bending when spring (22) deforms plastically in tension, while spring (21) deforms plastically in compression. The two cases when plastic compression occurs prior to buckling and when buckling occurs with springs ($i1$) compressed plastically but springs ($i2$) being compressed elastically, are described by Jones and dos Reis (1980) and Karagiozova and Jones (1992a), and are called "plastic-elastic" and "elastic-plastic" buckling, respectively. It should be noted that the initiation of static buckling occurs in the elastic range for the particular model studied which has a slenderness ratio of $L_1/L = 0.025$ ($h/l = 0.0125$) and the absorbed

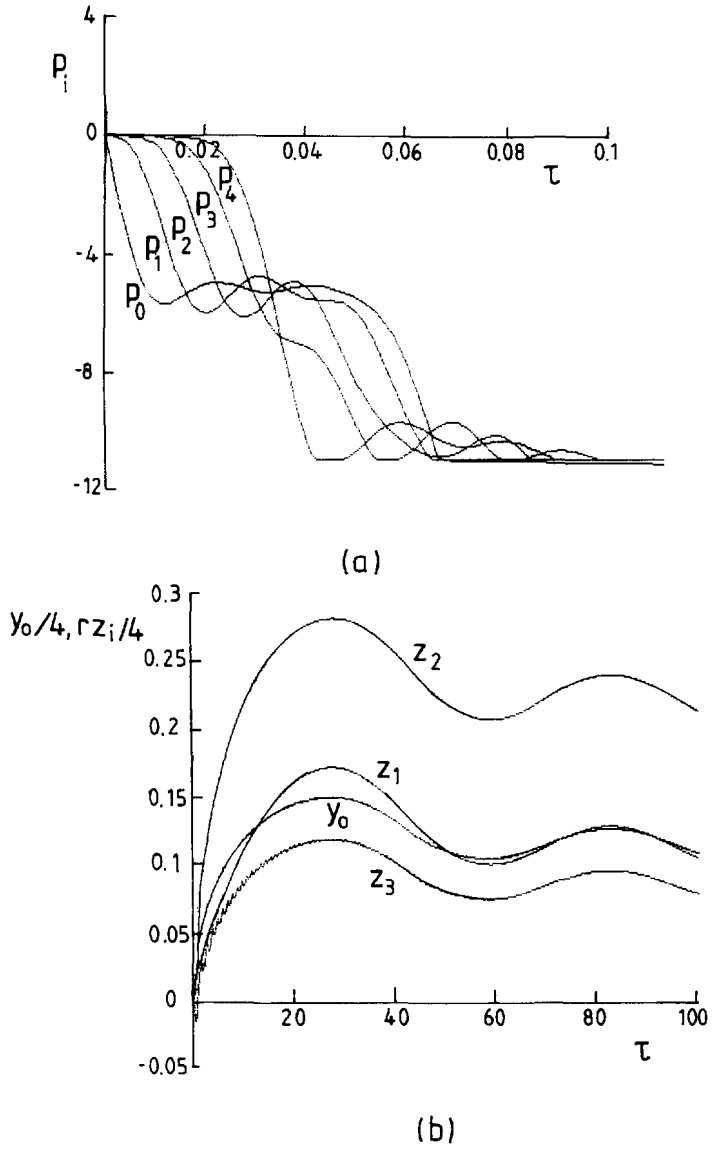

Fig. 6. Response of the model to an impact mass having $\mu = 100$ and $V_0 = 0.13$ ($r = 0.025$, $\lambda = 0.005$, $z_0 = 0.02$, $Q_{2x}^{1} = 5.447$). (a) Time delay of the dimensionless axial forces p_i; (b) temporal variation of the dimensionless axial displacement, u_0/l, and the dimensionless lateral displacements, ξ_i/l.

energy in subsequent post-bifurcation plastic deformations is due to the bending of the model only connected with compression in spring (21) and tension in spring (22).

5. LOWER BOUND TO THE INITIAL KINETIC ENERGY AND A CRITICAL BUCKLING ENERGY

The deformation process of the model in Fig. 1 when struck by a mass M with an initial velocity v_0 shows that both axial and lateral inertia effects play an essential role in the response. It is evident that the first phase of uniaxial compression is particularly significant for models subjected to sufficiently high impact velocities causing a uniform plastic compression of the springs and the absorption of a substantial proportion of the initial kinetic energy during the first phase.

The initial kinetic energy at the transition between the model response governed only by a uniform compression and the response of the model involving both compression and overall bending is a lower bound to the initial kinetic energy (LBE). In general, the lower bound to the initial kinetic energy is associated with the initiation of the dynamic instability

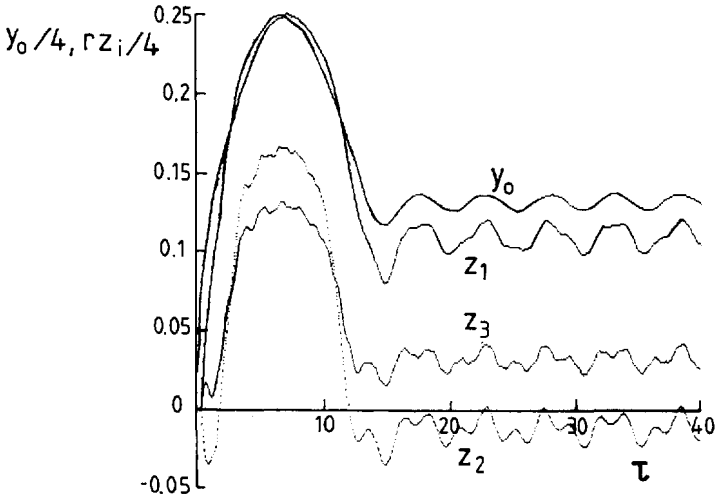

Fig. 7. Response of the model to an impact mass having $\mu = 6$ and $V_0 = 1.3$ ($r = 0.025$, $\lambda = 0.005$, $z_0 = 0.02$, $Q^*_{2\alpha} = 5.447$)—temporal variation of the dimensionless axial displacement, u_0/l, and the dimensionless lateral displacements, ξ_i/l.

(e.g. Lee (1977, 1981a, 1981b), Bell (1988)). For initial kinetic energies less than the LBE, a quasi-bifurcation does not occur and the response of the model is characterized by lateral vibrations ($z_i z_i'' < 0$) in a small neighbourhood of the initial undeformed position of the model, while the equilibrium state of the axial displacements is determined by the initial kinetic energy absorbed entirely in compression. The initial kinetic energy causing a loss of stability of the model is called a critical buckling energy (CBE).

The variation of the lower bound to the dimensionless initial kinetic energy and the dimensionless critical buckling energy with the mass ratio μ is shown in Fig. 9(a) and the variation of the dimensionless velocities corresponding to the above defined energies are shown in Fig. 9(b). The dashed curves in Figs 9(a,b) indicate the initial impact energies and velocities, respectively, when a quasi-bifurcation of the model response occurs in the elastic range. The regions 1, 2 and 3 in Fig. 9 indicate the load parameters which cause final buckling shapes of the model having characteristics of the first, second or third buckling modes, respectively.

The compression energy absorbed depends strongly also on the magnitudes of the initial imperfections. Models having large initial imperfections can absorb less compression energy than models having the same geometrical and material characteristics but smaller initial imperfections. Figure 10 shows the dimensionless initial kinetic energy which can be

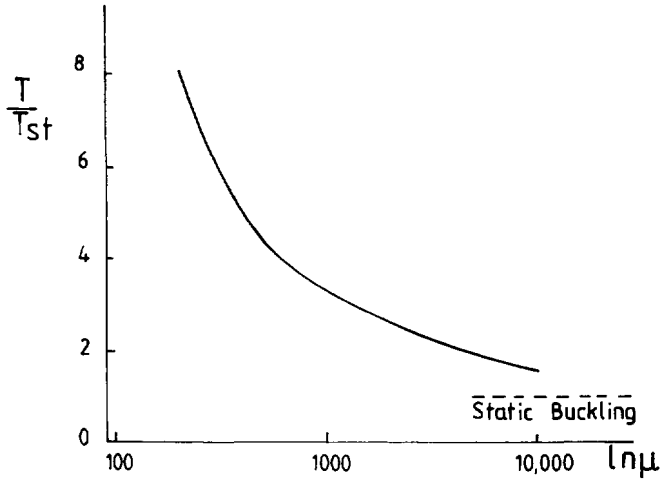

Fig. 8. Variation of the dimensionless buckling energy with the mass ratio, μ, for low velocity impact ($r = 0.025$, $\lambda = 0.005$, $z_0 = 0.02$, $Q^*_{2\alpha} = 5.447$).

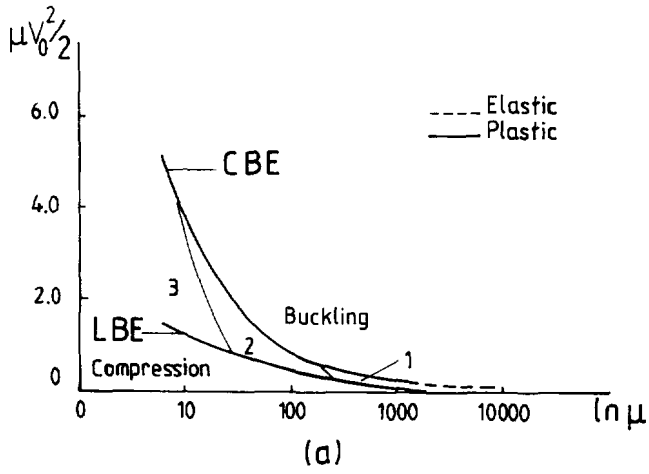

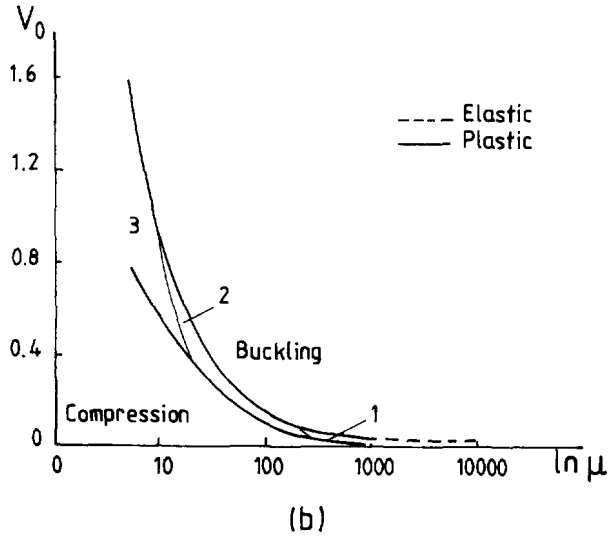

Fig. 9. (a) Variation of the lower bound to the dimensionless initial kinetic energy and the dimensionless critical impact energy with the mass ratio μ ($r = 0.025$, $\lambda = 0.005$, $z_0 = 0.02$, $Q_{iz}^{\flat} = 5.447$); (b) variation of the dimensionless velocities corresponding to the lower bound to the dimensionless initial kinetic energy and the critical impact energy with the mass ratio μ.

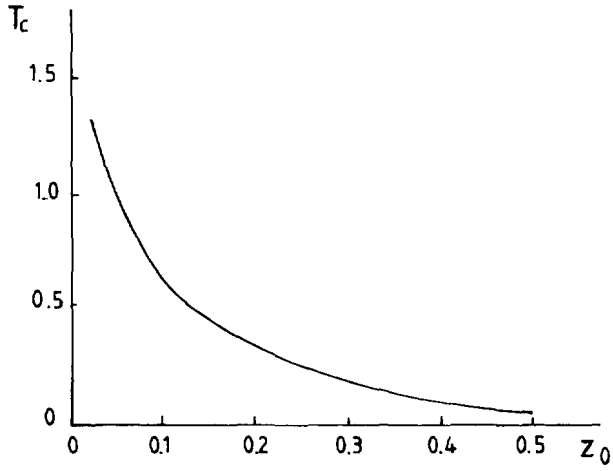

Fig. 10. Variation of the dimensionless initial kinetic energy absorbed during the compression phase with the dimensionless initial imperfections, z_0, for $\mu = 15$ and $V_0 = 0.72$ ($r = 0.025$, $\lambda = 0.005$, $Q_{iz}^{\flat} = 5.447$).

absorbed by the model with $\mu = 15$ when the response is governed only by compression, i.e., when no quasi-bifurcation occurs. It is evident that, for a constant mass ratio of $\mu = 15$, the energy absorbed decreases rapidly as the initial imperfections increase.

For initial kinetic energies lying between the LBE and the critical buckling energy, although a quasi-bifurcation occurs, the response of the model to an axial impact moves to a new but stable equilibrium state due to stiffness changes of the model after bifurcation. Several permanently deformed shapes of the model corresponding to stable post quasi-bifurcation states, for $\mu = 6$ and $\mu = 13$ and for different impact velocities V_0, are presented in Figs 11(a,b), respectively (the lateral displacements are exaggerated by a factor of two). It should be noted that, for the particular parameters considered, quasi-bifurcation occurs in the plastic flow regime for all initial kinetic energies between the LBE and the critical buckling energy. Figure 11(b) shows that different buckling mode shapes exist as post quasi-bifurcation equilibrium states for $\mu = 13$ and different impact velocities. It is evident that the deformed shape of the model has characteristics of the third buckling mode for $V_0 = 0.5$ and $V_0 = 0.6$, while a dimensionless impact velocity of 0.65 causes a buckled shape having characteristics of the second mode which is biased towards the impacted end. The dimensionless critical impact velocity $V_0 = 0.72$ also causes a deformed shape having characteristics of the second buckling mode. Such a response is due to the different distributions of the plastic deformations in compression before quasi-bifurcation has occurred. The plastic deformations in all of the springs of the model are similar for relatively low velocity impacts ($V_0 < 0.62$), while higher impact velocities cause larger compressive plastic deformations in those springs closer to the impacted end. Obviously, the distribution of the compressive plastic deformations plays an important role in the quasi-bifurcated mode but a more detailed study is required using higher degrees of freedom models.

The final buckling shapes of the model for several critical combinations (μ, V_0) are shown in Fig. 12. It is evident that an increase in the dimensionless critical impact velocity gives rise to a decrease in the dimensionless critical time of quasi-bifurcation. The critical combinations of the parameters in Fig. 12 show that the dimensionless initial momentum of the striking mass (μV_0) decreases from 13 to 8 with increase in velocity, while the dimensionless initial kinetic energy of the mass increases significantly from 0.845 to 6.4.

6. INITIATION OF BUCKLING—A COMPARISON BETWEEN THE MODEL PREDICTIONS AND BELL'S THEORY AND EXPERIMENTS

The initiation of buckling with large plastic strains predicted by the model in Fig. 1 can be compared with other theories and some experimental results in order to examine its applicability for actual impact problems. A criterion for the initiation of buckling is

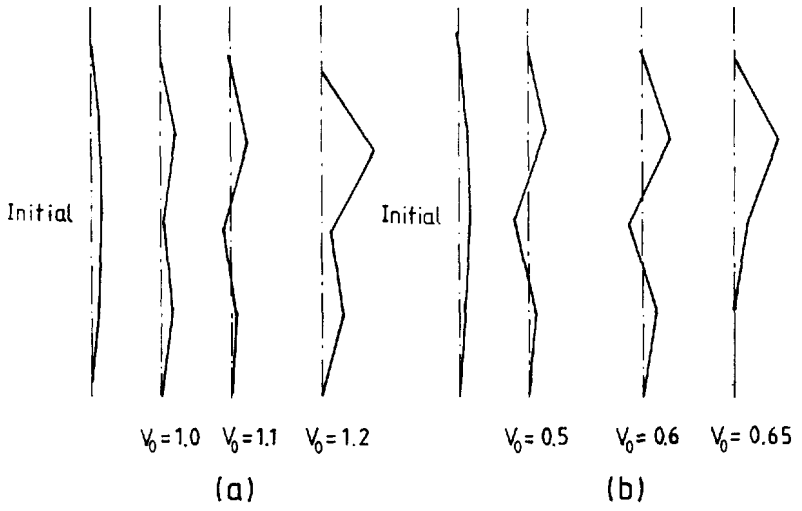

Fig. 11. Deformed shapes of the model corresponding to stable post quasi-bifurcation states ($r = 0.025$, $\lambda = 0.005$, $z_0 = 0.02$, $Q_{cr}^{\lambda} = 5.447$): (a) $\mu = 6$, (b) $\mu = 13$.

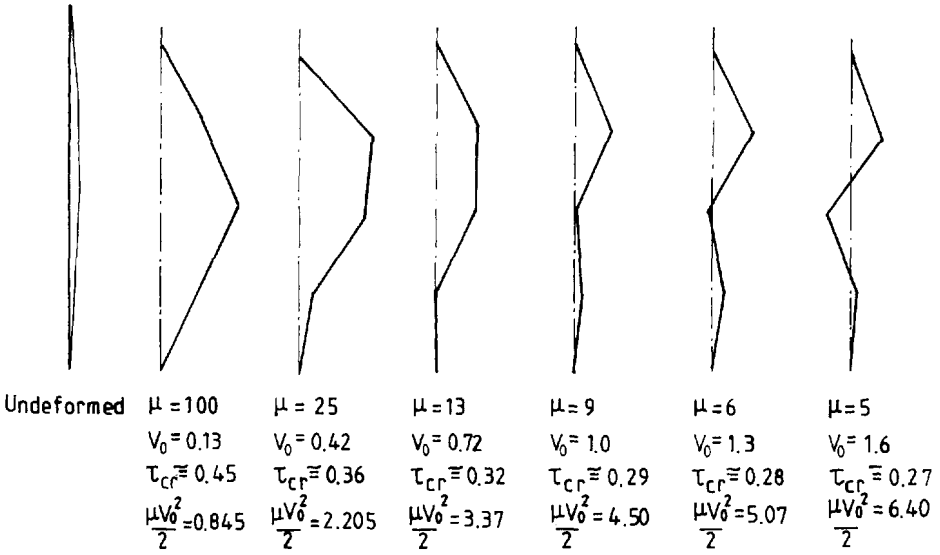

Fig. 12. Buckling shapes at several critical impact energies (the initial imperfections presented are exaggerated 125 times).

proposed by Bell (1988) using a quasi-static method of analysis for the dynamic axial plastic buckling of rods. The experiments reveal that the dynamic plastic buckling of a rod subjected to a free-flight impact originates with the arrival of the peak value of the plastic wave at a critical distance from the impact face. It is assumed that the region of the rod behind the peak stress of the propagating plastic wave front is one of constant stress, constant finite strain and constant particle velocity (Bell (1988)). Under these assumptions, the deformation state is considered as a quasi-static one and a critical length of buckling, L_{cr}, is determined from the condition

$$P_{cr} = [4n^2\pi^2(\mathrm{d}\sigma_x/\mathrm{d}\varepsilon_x)I]/L_{cr}^2. \tag{13}$$

where P_{cr} is the critical buckling load causing n semi-waves in a fully clamped section, $(\mathrm{d}\sigma_x/\mathrm{d}\varepsilon_x)$ is Engesser's tangent modulus and I is the moment of inertia for the cross-section. In order to predict the mode shape for an actual rod, it is necessary to note that the peak stresses in Bell's experiments (Bell (1988)) can only propagate a distance $0.43l$ (l is the length of a specimen) before being reduced through interaction with the reflected elastic wave front from the other end. Thus, if L_{cr} from eqn (13) lies within the range $0.215l \leqslant L_{cr} \leqslant 0.43l$ the rod suffers a single mode of deformation, whereas for $L_{cr} < 0.215l$, higher deformation modes would develop, e.g., the second mode would develop for $0.143l \leqslant L_{cr} \leqslant 0.215l$ and a third mode for $0.107l \leqslant L_{cr} \leqslant 0.143l$, approximately. Substituting $n = 1$ in eqn (13), the critical stress causing buckling of the bar is determined as

$$\sigma_{cr} = [4\pi^2(\mathrm{d}\sigma_x/\mathrm{d}\varepsilon_x)I]/(AL_{cr}^2), \tag{14}$$

where A is the cross-sectional area.

Several experiments were reported by Bell (1988) on the high velocity collision of identical aluminium bars. The associated deformation process in the particular case when the striking mass is equal to the mass of the struck specimen can be analyzed using the model in Fig. 1. The assumptions made by Bell (1988) correspond to the conditions when the phenomenon of quasi-bifurcation of the model occurs within the plastic flow regime (Sections 2–4). The impact behaviour of the model in Fig. 1 is restricted by the presence of four rigid links, so that only velocities causing buckling with a critical length larger than 1/4 can be considered.

The spring characteristics of the model in Fig. 1 which correspond to an annealed aluminium (Bell (1988)) with $\rho = 2730\ \mathrm{kg/m^3}$, $\sigma_0 = 30$ MPa, $E = 70$ GPa and $E_t = 1.2$ GPa

Table 1. Comparison between the experimental tests of Bell (1988), and the model predictions for annealed aluminium specimens having lengths of 35.6 cm and diameters of 2.14 cm ($r = 0.12$, $\sigma_x = \sigma_x(\max)$, $P = P_i(\max)$, $P^y = 2F_{i2}^y$)

Test	Experiment (Bell (1988))					Model		
	v_0, m/s	σ_x/σ_0	ε_x	L_{cr}, cm	t_{cr}, ms	P/P^y	ε_x	t_{cr}, ms
#855	40.3	3.01	0.054	10.2	0.155	2.55	0.0544	0.177
#860	30.0	2.53	0.040	11.8	0.179	2.18	0.0392	0.189
#863	40.7	3.04	0.055	10.2	0.155	2.57	0.0547	0.176
#864	44.5	3.20	0.062	9.6	0.145	2.75	0.0610	0.172
#867	43.6	3.17	0.061	9.6	0.145	2.70	0.0600	0.173
#877	48.5	3.40	0.070	9.0	0.136	2.93	0.0683	0.170

give elastic and plastic wave propagation speeds $c = 5060$ m/s and $c_p = 660$ m/s respectively. A comparison between the experimental results reported by Bell (1988) and the predictions of the model in Fig. 1 are obtained for the two specimens having a length of 35.6 cm and a diameter of 2.14 cm (Table 1), and a length of 25.4 cm with a diameter of 2.14 cm (Table 2). The comparison is made between the buckling initiation times, t_{cr}, the maximum strains, ε_x, and the ratio $\sigma_x(\max)/\sigma_0$ from the experiments which corresponds to the ratio $P_i(\max)/P^y$ for the model. The critical time for the experiments is taken as the time required for the plastic wave to travel a critical distance L_{cr}. The strain for the model is obtained approximately as $\varepsilon_i = \mathrm{d}u/\mathrm{d}x \cong (u_{i+1} - u_i)/L = (y_{i+1} - y_i)$.

It is evident that reasonable agreement is obtained between the theoretical predictions of the model and the corresponding experimental results although some differences are related to the simplifications inherent in the model. Good agreement is achieved between the maximum strains predicted by the model and the experimentally obtained values of ε_x and differences between 0.55% and 2.43% are observed for the specimens having $l = 35.6$ cm (Table 1) and differences up to 4.63% occur for the shorter specimens (Table 2). However, the stress-strain relationship in the theoretical analysis presented by Bell (1988) is a nonlinear one, while the springs in Fig. 1 are an idealization of an elastic-plastic material with linear strain hardening characteristics which results in larger differences between the predicted ratios P/P^y and the experimentally obtained ratios σ_x/σ_0. In general, the model in Fig. 1 predicts lower values of the maximum axial force which is between 13.82% (test #860) and 15.46% (Test #863) lower for the longer specimens (Table 1) and up to 9.48% (Test #1591) lower for the shorter ones (Table 2). The buckling initiation times in the tests are shorter than the critical times predicted by the model because the experimentally obtained critical lengths are shorter than the possible deformed lengths of the model. It is evident from Tables 1 and 2 that the agreement between the experimental results and numerical predictions is better for the lower impact velocities. As anticipated, it turns out that the limitation of four rigid links is quite a strong restriction for modelling the higher velocity impacts.

Based on the above discussion, it is evident that the initiation of buckling predicted by the model is in reasonable agreement with the buckling initiation reported by Bell (1988). A further increase in the degrees of freedom of the model could make possible a better comparison with the experimental results when the initiation of buckling occurs for shorter critical lengths.

Table 2. Comparison between the experimental tests of Bell (1988), and the model predictions for annealed aluminium specimens having lengths of 25.4 cm and diameters of 2.14 cm ($r = 0.1685$, $\sigma_x = \sigma_x(\max)$, $P = P_i(\max)$, $P^y = 2F_{i2}^y$)

Test	Experiment (Bell (1988))					Model		
	v_0, m/s	σ_x/σ_0	ε_x	L_{cr}, cm	t_{cr}, ms	P/P^y	ε_x	t_{cr}, ms
#1309	65.7	3.957	0.095	7.6	0.115	3.776	0.0925	0.122
#1591	66.9	4.218	0.108	7.2	0.101	3.820	0.1031	0.119
#1592	68.0	4.251	0.110	7.2	0.101	3.877	0.1050	0.117

It should be mentioned that although reasonable agreement is achieved for the initiation of buckling predicted by the model and the experimental results, it is difficult to compare the final buckling shapes. The theoretical analysis by Bell (1988), based on a quasi-static approach, does not consider the possibility of a large reduction in stiffness of the specimen during the post-buckling deformation. It was mentioned in Section 4 that the initial buckling mode can change due to a reduction in stiffness as buckling proceeds which produces final buckling shapes having longer semi-waves than the initial ones. In this connection, the discussion by Abrahamson and Goodier (1966) concerning a comparison between the experimental results and the theoretical analysis should be noted. It was mentioned by Abrahamson and Goodier (1966) that the predicted critical values of the buckling semi-waves are smaller than the experimentally observed ones and that this phenomenon was attributed to the variation of the hardening modulus during the buckling motion. However, the reported differences are between 20% and 200% so that it is likely that this phenomenon is related also to the stiffness changes of the specimen during the post-bifurcation deformation phase.

It turns out that a quasi-static analysis in the plastic range can predict only the dynamic buckling initiation but the final deformed shape cannot be predicted using such methods, unless the initial kinetic energies are small. Both the quasi-static method of analysis for the particular case $\mu = 200$, $V_0 = 0.06$ referred to in Section 4 (and also for larger values of μ) and Bell's quasi-static analysis would predict values which lie on the LBE curve in Fig. 9(a). The energies associated with the LBE curve are sufficient only for the initiation of buckling with no surplus energy for post-bifurcation behaviour and mode changes.

7. CONCLUSIONS

A multi-degrees of freedom model is used to study the phenomenon of dynamic elastic-plastic buckling when retaining the influences of axial and lateral inertia and the effects of initial geometrical imperfections. The proposed model follows the entire deformation history including several phases of elastic and plastic loading, unloading and reloading which makes possible the analysis of the post-bifurcation phenomenon.

The elastic-plastic bucking phenomenon is studied using the definition of quasi-bifurcation of an elastic-plastic discrete system introduced by Lee (1977, 1981a) together with an analysis of the post-bifurcation behaviour of the model.

It is found that the response of the model to an impact by a rigid mass travelling with an initial velocity consists of two distinct phases: a uniform axial compression followed by an overall bending. A delay in the spring loadings of the model due to the axial inertia effects is observed which is analogous to the uniaxial elastic and plastic wave propagation in a continuous body.

A lower bound to the initial kinetic energy causing a quasi-bifurcation of the model is defined as the initial kinetic energy at the transition between the model response when governed only by a uniform compression and a model response which involves overall bending as well as compression. The critical impact energy is defined as an energy causing a loss of dynamic stability of the model.

The final buckling shapes and the corresponding critical quasi-bifurcation times are determined for a model with a particular set of parameters and subjected to several impact mass ratios μ having initial impact velocities up to 46.5 m/s. Reasonable agreement is found between the critical quasi-bifurcation times predicted by the model and the corresponding experimental values for the high velocity collision of identical aluminium bars.

Some comments are also offered on the validity of a quasi-static method of analysis for the idealised model.

Further studies will be reported in due course on the response of higher degree of freedom systems which will clarify the axial wave propagation effects on the dynamic elastic-plastic buckling phenomenon and clarify further the range of validity of quasi-static methods of analysis.

Acknowledgments—The authors wish to record their gratitude to the British Council and the Bulgarian National Research Fund (Project MM-77/92) for supporting the collaboration between the Impact Research Centre in the

Department of Mechanical Engineering at the University of Liverpool and the Institute of Mechanics, Bulgarian Academy of Sciences. The authors are indebted to Mr. H. Parker for the preparation of the figures.

REFERENCES

Abrahamson, G. R. and Goodier, J. N. (1966). Dynamic flexural buckling of rods within an axial plastic compressive wave. *J. Appl. Mech.* **33,** 241–247.

Bell, J. F. (1988). The dynamic buckling of rods at large plastic strain. *Acta Mechanica* **74,** 51–67.

Gear, C. W. (1971). *Numerical Initial Value Problem in Ordinary Differential Equations*, Prentice-Hall, Englewood Cliffs, NJ.

Hartzman, M. (1974). Comparison of calculated static and dynamic collapse pressures for clamped spherical domes. *AIAA J.* **12,** 568–570.

Jones, N. and dos Reis, H. L. M. (1980). On the dynamic buckling of a simple elastic-plastic model. *Int. J. Solids Struct.* **16,** 969–989.

Jones, N. (1989). *Structural Impact*, Cambridge University Press, Cambridge, UK.

Karagiozova, D. and Jones, N. (1992a). Dynamic buckling of a simple elastic-plastic model under pulse loading. *Int. J. Non-Linear Mech.* **27,** 981–1005.

Karagiozova, D. and Jones, N. (1992b). Dynamic pulse buckling of a simple elastic-plastic model including axial inertia. *Int. J. Solids Struct.* **29,** 1255–1272.

Karagiozova, D. and Jones, N. (1993). Strain-rate effects in the dynamic buckling of a simple elastic-plastic model. *Impact Research Centre Report No ES/96/93*, The University of Liverpool.

Karagiozova, D. and Jones, N. (1995). Some observations on the dynamic elastic-plastic buckling of a structural model. *Int. J. Impact Engng* **16,** 621–635.

Lee, L. H. N. (1977). Quasi-bifurcation in dynamics of elastic-plastic continua. *J. Appl. Mech.* **44,** 413–418.

Lee, L. H. N. (1981a). Flexural waves in rods in axial plastic compressive wave. *Wave Motion* **3,** 243–255.

Lee, L. H. N. (1981b). Dynamic buckling of an inelastic column. *Int. J. Solids Struct.* **17,** 71–79.

Tam, L. L. and Calladine, C. R. (1991). Inertia and strain-rate effects in a simple plate-structure under impact loading. *Int. J. Impact Engng* **11,** 349–377.

APPENDIX

This appendix contains the details for determining the static buckling load and the natural frequencies of the lateral elastic vibrations for the model in Fig. 1. The relationships between some dimensional and dimensionless variables used for the idealised model are also presented.

A perfect model with $\xi_0 = 0$ can buckle statically at a load P_C which satisfies the following equations

$$-2\bar{M}_1 + \bar{M}_2 - P_C(-2\xi_1 + \xi_2) = 0,$$
$$\bar{M}_1 - 2\bar{M}_2 + \bar{M}_3 - P_C(\xi_1 - 2\xi_2 + \xi_3) = 0$$

and

$$\bar{M}_2 - 2\bar{M}_3 - P_C(\xi_2 - 2\xi_3) = 0, \tag{A1a–c}$$

where

$$\bar{M}_1 = KrL_1(2\xi_1 - \xi_2),$$
$$\bar{M}_2 = KrL_1(-\xi_1 + 2\xi_2 - \xi_3)$$

and

$$\bar{M}_3 = KrL_1(2\xi_3 - \xi_2), \tag{A2a–c}$$

when using, for the elastic case, $F_{ix} = KLx_{ix}$, $\bar{M}_i = -(F_{i1} - F_{i2})L_1/2$ together with eqns (4b–d).

Equations (A1) have a nonzero solution if

$$\begin{vmatrix} -(5KrL_1 - 2P_C) & 4KrL_1 - P_C & -KrL_1 \\ 4KrL_1 - P_C & -(6KrL_1 - 2P_C) & 4KrL_1 - P_C \\ -KrL_1 & 4KrL_1 - P_C & -(5KrL_1 - 2P_C) \end{vmatrix} = 0, \tag{A3}$$

which gives

$$(P_C)_1 = KrL_1(2 - \sqrt{2}), \quad (P_C)_2 = 2KrL_1, \quad \text{and} \quad (P_C)_3 = KrL_1(2 + \sqrt{2}). \tag{A4a–c}$$

Thus, the critical static buckling load for the model in Fig. 1 with $\xi_0 = 0$ is $P_C = KrL_1(2 - \sqrt{2})$.

The natural lateral elastic vibrations of the same model are governed by the equation

$$\mathbf{A}\ddot{\xi} + \mathbf{C}\xi = 0, \tag{A5}$$

where

$$[\xi]^T = [\xi_1,\ \xi_2,\ \xi_3],$$

$$\mathbf{A} = \begin{bmatrix} 2mL & 0 & 0 \\ 0 & 2mL & 0 \\ 0 & 0 & 2mL \end{bmatrix} \quad \text{and} \quad \mathbf{C} = \begin{bmatrix} 5KrL_1 & -4KrL_1 & KrL_1 \\ -4KrL_1 & 6KrL_1 & -4KrL_1 \\ KrL_1 & -4KrL_1 & 5KrL_1 \end{bmatrix}. \tag{A6a–c}$$

The corresponding frequency equation

$$\begin{vmatrix} -2mL\omega^2+5KrL_1 & -4KrL_1 & KrL_1 \\ -4KrL_1 & -2mL\omega^2+6KrL_1 & -4KrL_1 \\ KrL_1 & -4KrL_1 & -2mL\omega^2+5KrL_1 \end{vmatrix} = 0 \tag{A7}$$

determines the lateral elastic vibrations of the model in Fig. 1 as

$$\omega_1^2 = 8\sqrt{2}(4+3\sqrt{2})^{-1}Kr^2/m_1, \quad \omega_2^2 = 16Kr^2/m_1 \quad \text{and} \quad \omega_3^2 = 8(3+2\sqrt{2})Kr^2/m_1. \tag{A8a–c}$$

If the equality of the vibration frequencies ω_1^M and ω_1^A and the equality of the static buckling load for the model and the Euler buckling load for a column are used as criteria of equivalency between the model and an actual structure, then the relationship between the dimensionless time for the model, τ, and the dimensional time, t, for the structure becomes

$$\tau = \frac{\pi^2(2+\sqrt{2})^{1/2}cr}{32L\sqrt{6}}t, \tag{A9}$$

when using eqns (2f), (9), (12) and (A8a). Equation (A9) leads to a relationship between the dimensional impact velocity, v_0, and the dimensionless one, V_0, as

$$v_0 = \frac{\mathrm{d}u_0}{\mathrm{d}t} = \frac{\pi^2(2+\sqrt{2})^{1/2}cr}{32\sqrt{6}}V_0, \tag{A10}$$

when using eqn (2a).